AGU PUBLICATIONS

Geophysical Research Letters

RESEARCH LETTER
10.1002/2015GL064513

Key Points:
- Enhancement of solutes mixing in unsaturated porous media
- Mixing-induced reactivity in unsaturated porous media
- Vadose zone and gas-oil reservoir

Supporting Information:
- Texts S1 and S2 and Figures S1 and S2
- Figure S1
- Figure S2
- Data S1
- Texts S1 and S2 and Figure S1

Correspondence to:
J. Jiménez-Martínez and Y. Méheust,
jjimenez@lanl.gov;
yves.meheust@univ-rennes1.fr

Citation:
JimÉnez-MartÍnez, J., P. de Anna, H. Tabuteau, R. Turuban, T. Le Borgne, and Y. Méheust (2015), Pore-scale mechanisms for the enhancement of mixing in unsaturated porous media and implications for chemical reactions, *Geophys. Res. Lett.*, *42*, 5316–5324, doi:10.1002/2015GL064513.

Received 11 MAY 2015
Accepted 16 JUN 2015
Accepted article online 22 JUN 2015
Published online 14 JUL 2015

Pore-scale mechanisms for the enhancement of mixing in unsaturated porous media and implications for chemical reactions

Joaquín Jiménez-Martínez[1,2], Pietro de Anna[3], Hervé Tabuteau[4], Régis Turuban[1], Tanguy Le Borgne[1], and Yves Méheust[1]

[1]Geosciences Rennes, UMR 6118, CNRS, Université de Rennes 1, Rennes, France, [2]Now at Los Alamos National Laboratory, Los Alamos, New Mexico, United States, [3]Department of Civil and Environmental Engineering, Massachusetts Institute of Technology, Cambridge, Massachusetts, USA, [4]IPR, Université de Rennes 1-CNRS, UMR 6251, Rennes, France

Abstract Porous media in which different fluid phases coexist are common in nature (e.g., vadose zone and gas-oil reservoirs). In partially saturated porous media, the intricate spatial distributions of the wetting and nonwetting phases causes their flow to be focused onto preferential paths. Using a novel 2-D experimental setup allowing pore-scale measurement of concentration fields in a controlled unsaturated flow, we highlight mechanisms by which mixing of an invading fluid with the resident fluid is significantly enhanced when decreasing saturation. The mean scalar dissipation rate is observed to decrease slowly in time, while under saturated conditions it decays rapidly. This slow decrease is due to sustained longitudinal solute fingering, which causes concentration gradients to remain predominantly transverse to the average flow. Consequently, the effective reactivity is found to be much larger than under saturated conditions. These results provide new insights into the role that multiphase flows play on mixing/reaction in porous media.

1. Introduction

The mixing of solutes in unsaturated porous media flows (i.e., when at least two immiscible fluids or phases coexist) is a common process controlling solute concentrations and the associated reactivity in natural processes and industrial systems. This includes for instance rainwater infiltration in soils and related migration and dilution of diffuse or point source contaminants, artificial recharge and unconventional irrigation, enhanced oil recovery, geological storage of CO_2 or gases such as H_2, and nuclear waste storage. A decrease in the wetting phase (typically, water) content is known to modify the velocity distribution and thus the associated transport phenomena. In particular, it can lead to the development of regions of wetting fluid of very low velocities, including regions where it is trapped, and connected preferential channels of high velocity [*de Gennes*, 1983]. The dependence of the velocity field distribution on the saturation degree is expected to strongly impact solute transport, mixing, and chemical reactivity that take place within one of the immiscible phases (usually, the aqueous phase). The need to account for saturation-dependent mixing has been highlighted by studies focusing on the mixing of recently infiltrated water with "old" resident water in catchments [e.g., *Legout et al.*, 2007; *Brooks et al.*, 2009]. This effect has been quantified recently by introducing "ad hoc" dynamic partial mixing coefficients in catchment transport models [*Hrachowitz et al.*, 2013].

Numerous works have measured an increased dispersion when decreasing saturation [e.g., *Sato et al.*, 2003; *Nutzmann et al.*, 2002; *Maraqa et al.*, 1997; *Haga et al.*, 1999; *Padilla et al.*, 1999; *Toride et al.*, 2003; *Guillon et al.*, 2013; *Russo*, 1993; *Russo et al.*, 1994; *Russo*, 1995a; *Roth and Hammel*, 1996; *Raoof and Hassanizadeh*, 2013; *Wildenschild and Jensen*, 1999; *Bromly and Hinz*, 2004]. Furthermore, the increase of flow heterogeneity with water desaturation has been shown to lead to dispersion processes that are non-Fickian to a larger extent [e.g., *Wildenschild and Jensen*, 1999; *Bromly and Hinz*, 2004; *Guillon et al.*, 2013], in particular in relation to mobile-immobile mass transfer processes described by nonequilibrium models, such as dual-continuum [*Nielsen et al.*, 1986; *Simunek and van Genuchten*, 2008] or Continuous Time Random Walks (CTRW) representations [e.g., *Cortis and Berkowitz*, 2004; *Zoia et al.*, 2010]. Although the mechanisms behind this change in dispersion regime are well understood, the explicit relationship between saturation and the non-Fickian transport parameters is still largely debated and likely nonuniversal [e.g., *Sahimi*, 2012]. While all these studies, mainly from laboratory experiments in disturbed or repacked soils,

Table 1. Main Control Parameters, for the Investigated Saturation Degrees S_w: Flow Q, Mean Velocity $\bar{v}$, Reynolds (*Re*), Péclet (*Pe*), and Capillary (*Ca*) Numbers

S_w	Q (mm^3 s^{-1})	$\bar{v}$ (mm s^{-1})	*Re* (-)	*Pe* (-)	*Ca* (-)
1.0	0.55	0.017	$5.49 \cdot 10^{-4}$	54	
1.0	1.375	0.043	$1.37 \cdot 10^{-3}$	135	
0.7	0.55	0.025	$7.87 \cdot 10^{-4}$	78	$2.04 \cdot 10^{-5}$
0.6	0.55	0.029	$9.18 \cdot 10^{-4}$	91	$2.38 \cdot 10^{-5}$

indicate an enhancement of dispersion when decreasing saturation, the opposite behavior, mainly from experiments in natural-undisturbed soils, has also been observed [e.g., *Hammel and Roth*, 1998; *Russo*, 2005; *Vanderborght and Vereecken*, 2007]. This phenomenon is explained in particular by the fact that an increase in saturation can correspond to an increase in flow rates, which induces larger velocity fluctuations for some soil structures. For anisotropic media it has also been observed that the effect of saturation on dispersion is dependent on the orientation of the mean flow direction with respect to the heterogeneities [e.g., *Russo*, 1995b; *Russo et al.*, 1998].

Unsaturated flows thus exhibit a rich scope of transport behaviors, which have been explored so far mainly through the analysis of solute-spreading properties. While the characterization of solute spreading is important to predict the spatial extent of solutes plumes or the distribution of transfer times in porous media, it does not directly inform about the actual mixing of solutes and the concentration distribution affecting chemical reaction processes [e.g., *Fluhler et al.*, 1996; *de Barros et al.*, 2012; *Chiogna et al.*, 2012; *de Anna et al.*, 2014a]. Mixing, in contrast, quantifies the distribution of concentration gradients within solutes plumes; these gradients control diffusive mass transfer and thus the evolution of concentration distributions [e.g., *Ottino*, 1989; *Kitanidis*, 1994; *Dentz et al.*, 2011]. While spreading and mixing are directly coupled, as spreading generally enhances mixing, the relationship between them is not direct [e.g., *Dentz et al.*, 2011]. In particular, a transport model fitting a breakthrough curve cannot, in general, predict chemical reactions resulting from solute mixing within the plume, since chemical reactions depend nonlinearly on concentration fluctuations which are not resolved by dispersion models [e.g., *Battiato et al.*, 2009]. While the number of studies addressing dispersion in unsaturated flows is significant, there has been much less work specifically targeting mixing processes and their consequences for chemical reactions under these conditions. A common view is that the existence of more pronounced preferential flow paths in unsaturated flow should induce faster traveltimes and thus decrease the time for solute mixing and chemical reactions [e.g., *Vanderborght et al.*, 2001; *Ursino et al.*, 2001; *Persson et al.*, 2005]. As discussed in the current study, this perception is not always correct as flow channeling may also increase concentration gradients and thus diffusive mass transfer and consequent reaction rates.

In this letter we quantify the impact of water saturation on mixing through novel pore-scale experimental imaging of solute concentrations in unsaturated flows. While most past studies have focused on Darcy scale heterogeneities, the presented experimental setup offers a pore-scale vision of transport processes, which is particularly relevant to the study of chemical reactions that depend nonlinearly on the microscale concentration distribution. We find that the formation of preferential flow paths in unsaturated flows largely enhances the mixing rate, and, consequently, the chemical reactivity, quantified here for large Damköhler number. In contrast to what is observed under saturated conditions, concentration gradients are found to be sustained in the direction transverse to the average flow through a coupling between non-Fickian longitudinal dispersion and diffusion into immobile zones transverse to preferential flow channels. Hence, these results uncover new mechanisms for the control of saturation on mixing and reaction processes.

2. Materials and Methods

The experimental flow cell is based on a horizontal analogous two-dimensional (2-D) porous medium consisting of a monolayer of cylindrical grains. The experimental setup allows capturing the incomplete mixing occurring within the pores from the measurement of (i) the solute concentration field in the liquid (wetting) phase [*de Anna et al.*, 2014b] and (ii) the spatial distribution of the two fluid phases (wetting and nonwetting).

The wetting fluid used is a 60–40% by weight *water-glycerol* solution dyed with Fluorescein, while *air* is used as nonwetting fluid; the viscosity ratio between the two fluids is 10^{-3}. In horizontal immiscible two-phase flows, the geometrical arrangement of the phases is controlled by the viscosity contrast between the two fluids

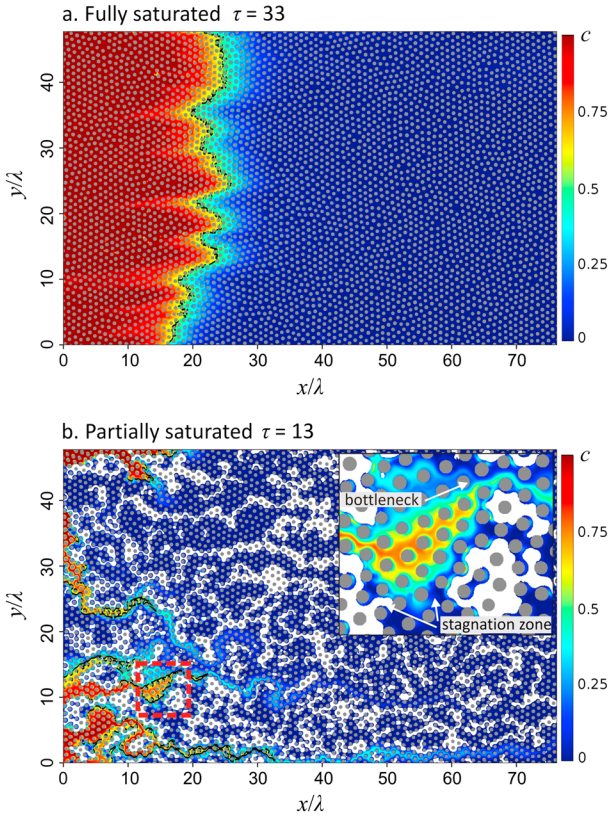

Figure 1. (a) Normalized concentration field $c(\boldsymbol{x}, \tau)$ obtained in fully saturated conditions at $\tau = t/t_a = 33$; it shows the concentration field with the centerline Γ superimposed in black. (b) $c(\boldsymbol{x}, \tau)$ under partially saturated conditions ($S_w = 0.7$) at $\tau = 13$. In stagnation zones the tracer is diffused, while at bottlenecks formed between air clusters, coalescence of tracer fingers takes place.

[*Lenormand*, 1990], the average displacement velocity [*Lenormand*, 1990; *Løvoll et al.*, 2004; *Toussaint et al.*, 2012], and how the fluids are injected into the medium. Here we obtain the phase geometry by injecting the two fluids together, in a manner similar to that of *Tallakstad et al.* [2009]; this method provides the possibility of imposing a spatially homogeneous saturation degree (in a statistical sense) with a geometric configuration of the phases that is realistic. A detailed description of the model dimensions, fluid properties (wetting and nonwetting phase), and experimental protocol is given in the supporting information.

The flow and transport regimes are characterized by four dimensionless numbers (Table 1). The wetting saturation S_w is the fraction of the total pore volume occupied by clusters of the wetting fluid. The Reynolds number, which compares the typical ratio of inertial forces to viscous forces, is $Re = \rho_w \bar{v} a/\mu_w$, where ρ_w is the density, $\bar{v}$ the average flow velocity, μ_w the viscosity of the wetting phase, and a the average pore throat. The capillary number, which quantifies the relative magnitude of viscous to capillary forces, is expressed as $Ca = \mu_w Q a^2/(\gamma \kappa A)$, where Q is the flow rate, γ the surface tension at the interface between the two fluid phases, κ the absolute permeability, and A the cross-sectional area in the direction normal to the average flow direction [e.g., *Méheust et al.*, 2002]. The Péclet number, which characterizes the relative importance of advective and diffusive effects during transport, is $Pe = \bar{v} a^2/(2D\lambda)$, where D is the molecular diffusion coefficient and λ the average pore size. Note that in this experimental setup the flow rate is decoupled from the water saturation. Hence, the two variables can be varied independently over a certain range. This is different from common Darcy scale experimental setups where the flow rate increases with saturation [e.g., *Vanderborght et al.*, 2001].

3. Results and Discussion

3.1. Concentration Fields

A snapshot of the concentration field of the invading fluorescent tracer, both under fully and partially saturated conditions is shown in Figure 1 for the same injection flow rate ($Q = 0.55$ mm^3 s^{-1}). The injected solution has a homogeneous nondimensional concentration $c = 1$ (see supporting information). The geometry of the mixing zone (where $0 < c < 1$) can be characterized by (i) its longitudinal extension σ (longitudinal standard deviation of the mean concentration), which quantifies the spreading of the invading solution within the host medium, and (ii) the length Σ of its center line Γ, defined as the set of locations at which $c = 1/2$. We shall call Γ the interface between the two solutions, though it is in effect the center line of a diffuse interface.

In the saturated case, $\sigma(t)$ increases approximately diffusively, as $t^{1/2}$ (data not shown here). In the unsaturated case, the presence of the air leads to a highly channelized flow, with large stagnation zones developing between air clusters. This broad distribution of velocities is expected to result in a superdiffusive spreading $\sigma(t)$ of the solute [e.g., *Wildenschild and Jensen*, 1999; *Bromly and Hinz*, 2004; *Cortis and Berkowitz*, 2004; *Zoia et al.*, 2010; *Guillon et al.*, 2013], associated to a flow organization in well-developed fingers (Figure 1) along

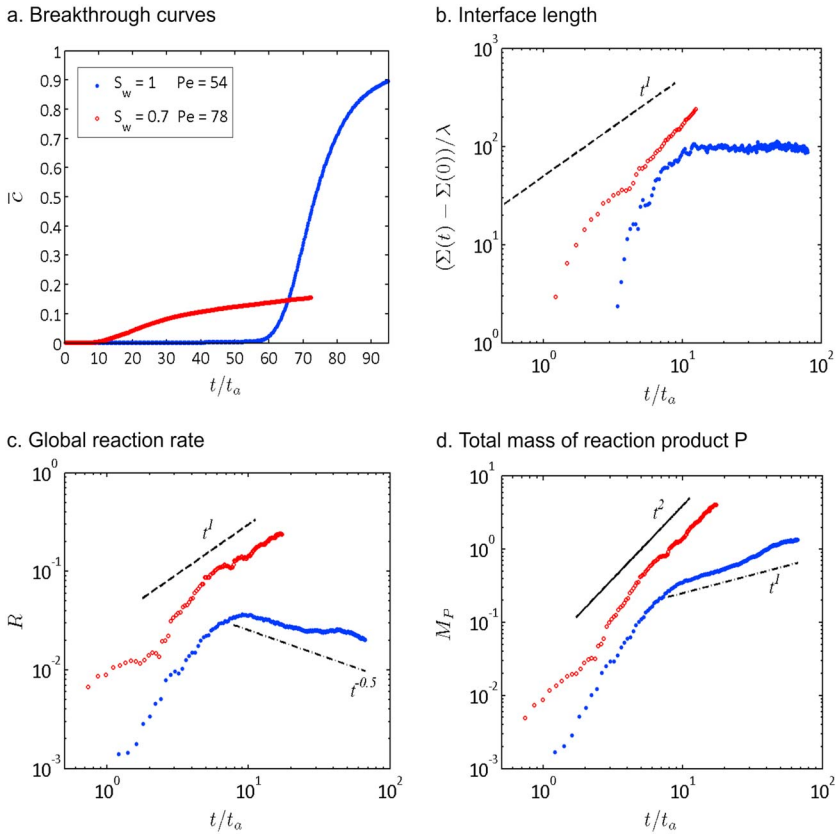

Figure 2. (a) Breakthrough curves (BTCs) measured at $x/\lambda = 63$ for fully saturated ($S_w = 1$ blue dots) and partially saturated conditions ($S_w = 0.7$ red circles). (b) Temporal evolution of $\Sigma - \Sigma(0)$, where Σ is the length of the center line Γ. (c) Temporal evolution of the global reaction rate R, which is obtained from the spatial integration of the local reaction rate r. (d) Total mass of reaction product, M_P; it is obtained from the temporal integration of R (see supporting information).

which the concentration gradient develops mainly in the direction transverse to the average flow. A measure of the impact of that spatial organization on solute transport is given by the breakthrough curves: under partially saturated conditions they are strongly asymmetric, with earlier breakthrough and much longer tailing than their saturated counterpart (Figure 2a).

The finger structure developed in the unsaturated cases also leads to a significant increase of the surface available for fluid mixing [e.g., *Jha et al.*, 2011]. This is visible in the temporal evolution of the interface length Σ in Figure 2b. In the saturated case, Σ initially increases and then stabilizes to a plateau value. The initial increase corresponds to the entrance of the mixing front into the porous media domain and its stretching by the flow heterogeneity [*Le Borgne et al.*, 2013]. This initial transient, also observed in experiments by *de Anna et al.* [2014b] in saturated conditions, disappears when finger merge transversally through diffusion, making the length of the mixing interface cease to increase. On the other hand, for partially saturated conditions, Σ increases faster than linearly in time (Figure 2b) and does not reach a plateau. Even though some finger coalescence does occur in bottlenecks, where flow lines are focused between air clusters (Figure 1b), that linear increase prevails through the continuous creation of new fingers. The strong deformation of the mixing interface, and the consequent enhancement of mixing, is analogous to observations made in Darcy scale heterogeneous flow topologies in saturated porous media [*de Barros et al.*, 2012; *Le Borgne et al.*, 2014].

This phenomenology was confirmed for different saturations and different Péclet numbers (see supporting information).

3.2. Mixing-Induced Reactivity $A + B \rightleftharpoons P$

In order to analyze the impact of saturation on chemical reactivity, we derive estimates of the local reaction rates that would be observed if the mixing of an injected liquid and a resident liquid, miscible with each other,

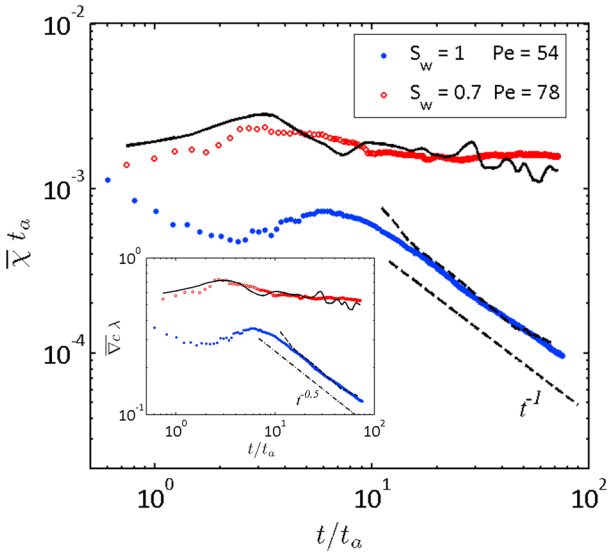

Figure 3. The main figure displays the time evolution of the mean scalar dissipation rate $\overline{\chi}(t)$ under fully ($S_w = 1$ blue dots) and partially saturated ($S_w = 0.7$ red circles) conditions. The insets shows the time evolution of the mean concentration gradient $\overline{\nabla c}(t)$. Estimates of $\overline{\chi}(t)$ from equation (4) are plotted for fully and partially saturated conditions as dotted and continuous line, respectively.

triggered a fast reversible reaction, i.e., a reaction (of characteristic timescale t_r) that is quasi-instantaneous with respect to advective mechanisms (of characteristic timescale t_a), that is, of Damköhler number $Da = t_a/t_r \gg 1$ [e.g., *Le Borgne et al.*, 2014]. For this we use the method presented by *de Simoni et al.* [2005, 2007] and *Willmann et al.* [2010], which allows quantifying the spatial distribution of local reaction rates r from the measured conservative concentration fields $c = c_A - c_B$ for a fast reversible reaction of known equilibrium constant K (see supporting information), according to the following relation:

$$r = \frac{2K}{(c^2 + 4K)^{3/2}} D \|\nabla c\|^2, \qquad (1)$$

where $\| \|$ denotes the vector magnitude.

The largest reaction rates are expected to be localized in areas of large concentration gradients. Hence, the spatial structure of concentration gradients is found to significantly impact the upscaled reactivity, i.e., the global reaction rate R, computed as the integral over the entire spatial domain of r (Figure 2c). In particular, while under saturated conditions the global reaction rate decreases after an initial increase, under unsaturated conditions its increase rate keeps approximately constant over the observation time (before mass starts leaving the domain). The late time reaction rate is higher in the unsaturated cases than in the saturated ones, even though we can only investigate times that are half a decade smaller due to the faster solute breakthrough. This translates directly into a large difference in the mass of the reaction product, M_P (Figure 2d). This behavior was confirmed for different saturations and different Péclet numbers (see supporting information).

The impact of mixing on the reaction rate is quantified through the product of the diffusion coefficient with the squared conservative concentration gradient (see supporting information). The integration of this term over the domain represents the scalar dissipation rate of concentration gradients [e.g., *Ottino*, 1989; *Le Borgne et al.*, 2010]. Thus, the temporal behavior of the global reaction rate is tightly linked to that of the scalar dissipation rate. In order to understand this behavior quantitatively, we analyze in details the dynamics of the concentration gradients in what follows.

3.3. Temporal Dynamics of Concentration Gradients

Figure 3 shows the temporal evolution of the mean concentration gradient $\overline{\nabla c}(t)$ and the mean scalar dissipation rate $\overline{\chi}(t)$ over the diffuse mixing interface, defined respectively as,

$$\overline{\nabla c} = \frac{1}{S_m} \int_{\Omega_m} dx\, dy\, \|\nabla c\| \qquad (2)$$

and

$$\overline{\chi} = \frac{1}{S_m} \int_{\Omega_m} dx\, dy\, D\|\nabla c\|^2. \qquad (3)$$

where S_m is the area of the mixing zone Ω_m defined as $\Omega_m = \{(x,y)|0.05 < c(x,y) < 0.95\}$.

In the fully saturated case and for different flow rates, the mean concentration gradient decays at large times after an initial quasi-constant transient. This scaling is in the form $\overline{\nabla c} \sim 1/\sqrt{t}$, as shown by the blue curve in Figure 3 (inset). This behavior is explained by the Fickian increase of the longitudinal dispersion length σ (see Figure 1) in the saturated medium. Indeed, after coalescence of early time fingers, the concentration

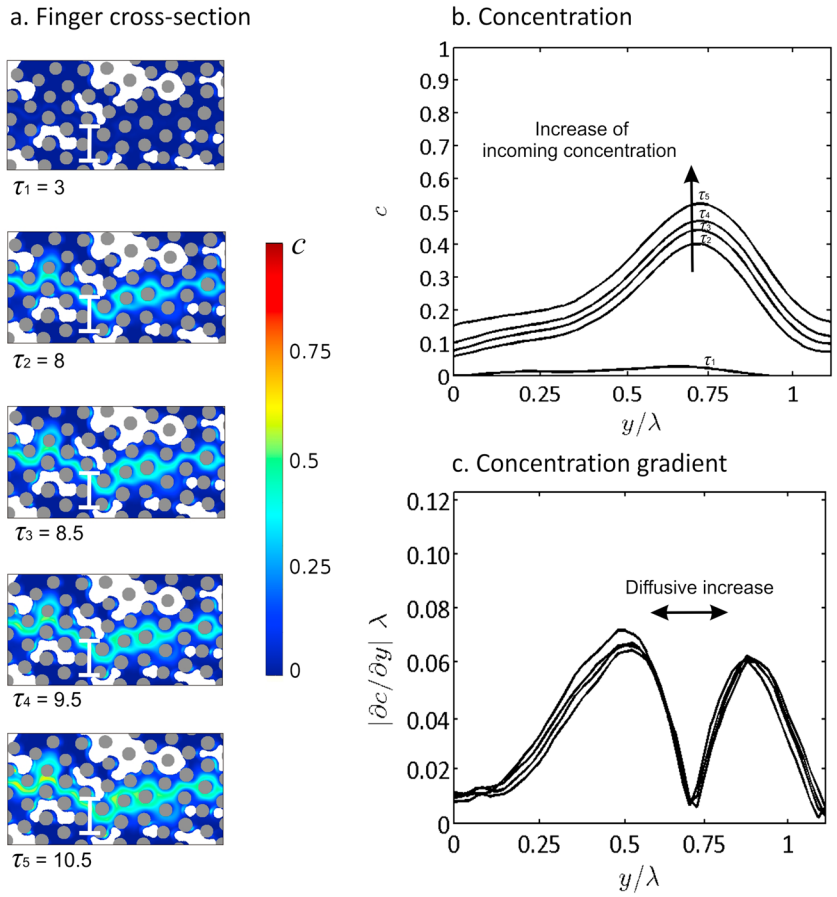

Figure 4. (a) Snapshots of one finger at different times ($\tau_i = t_i/t_a$) for a partially saturated test ($S_w = 0.7$). (b) Concentration profile along the vertical white segment indicated in the snapshots in Figure 4a, at different times. An increase of the incoming concentration is observed. (c) Profile of the concentration gradient $|\partial c/\partial y|$ at different times; $|\partial c/\partial y|$ is the absolute value of the derivative of the profile shown in Figure 4b. The direction of the diffusive widening of the figure is indicated by an arrow.

gradients are mostly oriented along the longitudinal direction. Hence, the mean concentration gradient may be approximated as $\overline{\nabla c} \approx 1/\sigma \sim 1/\sqrt{t}$, which provides a good prediction of the temporal evolution of $\overline{\nabla c}$ for saturated porous media at late times. Note that the early time behavior, controlled by a short initial fluid stretching regime, could also be modeled by a lamella-based model [e.g., *Le Borgne et al.*, 2013; *de Anna et al.*, 2014a].

In the partially saturated cases, $\overline{\nabla c}$ is always larger than in the saturated cases and decays slowly in time as shown by the red curve in Figure 3. This persistence of large concentration gradients is at the origin of the enhancement of chemical reactivity. In contrast to the saturated cases, concentration gradients are mostly oriented along the direction transverse to the average flow (Figure 1b). Elongated tracer fingers carry high concentrations that diffuse laterally into less mobile regions (see Figure 1b). Therefore, in the case of transport by an unsaturated flow, considering the concentration field at time t, we can approximate the characteristic transverse gradient at longitudinal position x in a finger as $\|\nabla c\|(x,t) \simeq 2\, c_f(x,t)/w_f(x,t)$, where c_f is the maximum finger concentration at x and $w_f/2$ is the finger half width at x. While the lateral finger size is expected to grow through diffusion, the maximum finger concentration c_f increases slowly in time as the result of the important longitudinal dispersion and the mixing processes (i.e., interaction with other fingers) upstream of location x (Figure 1b). In particular, critical bottlenecks (Figure 1b), which are known to focus a large part of the flow in unsaturated porous media [*de Gennes*, 1983], favor the coalescence of fingers with different mean velocities, thus leading to a slow increase of the downstream concentrations. This persistent slow increase of the maximum concentration is thus concomitant with a slow increase of the finger width w_f, leading to an approximately constant gradient over a large range of times (Figure 4).

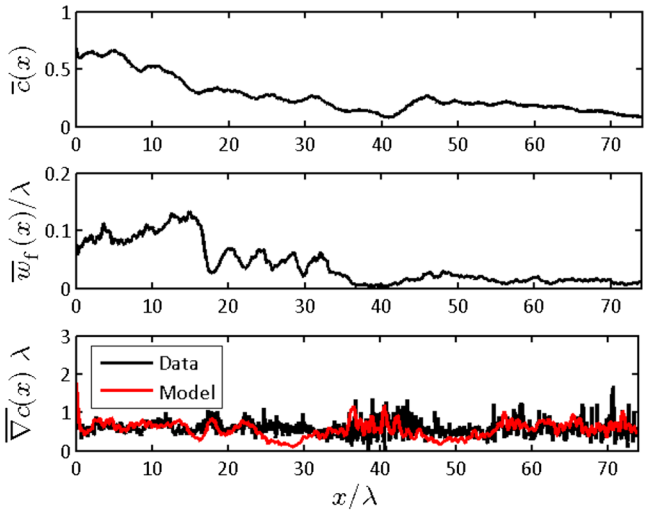

Figure 5. Dependence on x of the (top) mean concentration $\overline{c}(x,t) \simeq \overline{c}_f(x,t)$ and (middle) typical finger width $\overline{w}_f(x,t))$, for the concentration field of Figure 1b ($t/t_a = 13$). (bottom) The corresponding estimate of the average concentration gradient, $\overline{\nabla c} = 2\,\overline{c}_f/\overline{w}_f$, is compared to values obtained from a direct calculation.

3.4. The Role of Fingered Transport and Non-Fickian Dispersion on Mixing in Unsaturated Flows

As discussed above, we identify three main processes controlling mixing at the pore scale in unsaturated porous media: advective fingering, transverse diffusive mass transfer, and finger coalescence (Figures 1b and 4). In contrast to what is observed under saturated conditions [*Le Borgne et al.*, 2013; *de Anna et al.*, 2014a], continuous transverse coalescence of the solute fingers is limited by the presence of air clusters, so that no regime where concentration gradients are mostly longitudinal is observed; the concentration gradients remain mostly transverse to the average flow.

To quantify these mechanisms, we propose to estimate the concentration gradient averaged over the transverse direction y as $\overline{\nabla c}(x,t) \simeq 2\,\overline{c}_f(x,t)/\overline{w}_f(x,t)$, where the overline $\left(\overline{\ }\right)$ is to be understood as a an average over Ω_m and along the y only (see supporting information for details); this notation is identical to that of the global average used in equations (2) and (3), so to avoid any ambiguity, we indicate the space and time dependencies for all quantities mentioned below. We estimate the two factors $\overline{c}_f$ and $1/\overline{w}_f$ independently from the images and confirm the validity of this approximation (Figure 5). Note that $\overline{c}_f(x,t)$ is approximated as the average concentration in the mixing zone at longitudinal position x, $\overline{c}(x,t)$ (see supporting information for the detailed estimation of $\overline{c}_f$ and $\overline{w}_f$). Hence, the persistence of large concentration gradients can be understood from the ingredients presented in section 3.3, and consequently results from the spatial distribution and temporal dynamics of the two factors. The average concentration $\overline{c}(x,t)$ decays smoothly with the longitudinal position and differs from the profile observed for the saturated case. This is a characteristics of non-Fickian dispersion arising from the partially saturated conditions. As illustrated in Figure 1b, the high-velocity flow paths carry most of the tracer quickly through the domain, while the concentration increases slowly close to the inlet as the tracer invades the low-velocity regions. As expected, the typical finger width at longitudinal position x, $\overline{w}_f(x,t)$, is larger close to the inlet, where some of the stagnation zones have been invaded, than at the edge of the plume, where only fingers carry tracer. As both $\overline{c}$ and $\overline{w}_f$ decrease weakly with the distance from the tracer inlet, the average concentration gradient appears to depend only weakly on the longitudinal position. This is again in contrast to the saturated case where concentration gradients are localized in the mixing zone corresponding to the dispersing front.

We obtain an estimation of the global average concentration gradient, $\overline{\nabla c}(t)$, by integrating $\overline{\nabla c}(x,t)$ along the system length L, with a local weighting by the transverse extent of the mixing zone at position x and a normalization by the area of the mixing zone, S_m (see supporting information for details). This calculation yields

$$\overline{\nabla c}(t) = \frac{2}{S_m(t)} \int_0^L \mathrm{d}x\, \overline{c}(x,t)\, n_f(x,t), \tag{4}$$

where $n_f(x,t)$ is the typical number of fingers at longitudinal position x in the image recorded at time t.

This expression compares well with the direct measurement of $\overline{\nabla c}(t)$ (Figure 3), which validates our assumption that concentration gradients remain mainly transverse to the average flow under unsaturated conditions. Since the variance of the concentration gradient distribution, $\sigma^2_{\nabla c}$, can be computed as $\overline{(\nabla c)^2} - (\overline{\nabla c})^2$, the average scalar dissipation rate can simply be estimated from the average concentration gradient as $\overline{\chi} = D\left(\overline{\nabla c}^2 + \sigma^2_{\nabla c}\right)$. As $\sigma^2_{\nabla c}$ is found to be much smaller than the average concentration gradient squared, we use the simple approximation $\overline{\chi} \approx D\overline{\nabla c}^2$, where the average concentration gradient is given by equation (4). This relation provides a good estimate of the temporal evolution of the scalar dissipation rate over the range of investigated times (Figure 3). The persistence of large scalar dissipation rates in unsaturated porous media is thus the result of the finger dynamics (longitudinal finger development, transverse molecular diffusion, and occasional finger coalescence) as well as of the non-Fickian solute dispersion, which controls the concentration carried by fingers.

4. Conclusion

The presented experimental results shed new light on pore-scale mixing processes in unsaturated porous media. In particular, we uncover a basic mechanism by which mixing rates are significantly enhanced under unsaturated conditions. The first ingredient responsible for enhanced mixing is the formation of a ramified finger structure, shaped by the distribution of air clusters, which creates a large interface available for diffusive mass transfer. The second important process controlling mixing is non-Fickian dispersion, which leads to a persistent slow increase of finger concentrations, sustaining large concentration gradients. The third process is the limitation of finger merging by air clusters. These three processes induce concentration gradients that remain mainly normal to the average flow direction. Indeed, an estimate of the mean concentration gradient, $\overline{\nabla c}$, and mean scalar dissipation rate, $\overline{\chi}(t)$, based on these assumptions and from the measured finger width and mean concentration in fingers, compares well with direct measurements of $\overline{\nabla c}$ and $\overline{\chi}(t)$. Lowering the saturation and porous medium heterogeneity is expected to enhance flow fingering as a consequence of larger flow localization along better defined preferential flow paths and therefore also enhance mixing and reactivity.

We expect this mechanism to play an important role in controlling dilution and reaction processes in the vadose zone as well as in other natural and industrial systems. Though mixing enhancement is demonstrated here at the pore scale, we can postulate that it is expected to occur in unsaturated porous media where the above mentioned main ingredients are present. It could therefore be relevant at larger scales, depending on the medium geometry. But given the role played by air clusters, this mechanism of mixing enhancement would probably be efficient at scales not much larger than the size of the larger air clusters in the system. In our two-dimensional setup, the phase geometry exhibits no typical size for the air clusters, and the largest clusters are on the order of the system size [*Tallakstad et al.*, 2009], which makes the mixing enhancement particularly efficient.

Acknowledgments

J.J.-M. expresses his gratitude to Fondation Rennes 1. Y.M. acknowledges support from Rennes-Métropole through an A.I.S. grant from equipment. The authors gratefully acknowledge support from INSU/CNRS through the EC2CO program, under project AO2014-906387. The experimental work was also supported by the Interreg project CLIMAWAT, EU-RDF INTERREG IVA France (Channel)-England program.

The Editor thanks two anonymous reviewers for their assistance in evaluating this paper.

References

Battiato, I., D. M. Tartakovsky, A. M. Tartakovsky, and T. Scheibe (2009), On breakdown of macroscopic models of mixing-controlled heterogeneous reactions in porous media, *Adv. Water Res.*, *32*(11), 1664–1673.

Bromly, M., and C. Hinz (2004), Non-Fickian transport in homogeneous unsaturated repacked sand, *Water Resour. Res.*, *40*, W07402, doi:10.1029/2003WR002579.

Brooks, J. R., H. R. Barnard, R. Coulombe, and J. J. McDonnell (2009), Ecohydrologic separation of water between trees and streams in a Mediterranean climate, *Nat. Geosci.*, *3*, 100–104.

Chiogna, G., D. Hochstetler, A. Bellin, P. Kitanidis, and M. Rolle (2012), Mixing, entropy and reactive solute transport, *Geophys. Res. Lett.*, *39*, L20405, doi:10.1029/2012GL053295.

Cortis, A., and B. Berkowitz (2004), Anomalous transport in classical soil and sand columns, *Soil Sci. Soc. Am. J.*, *68*, 1539–1548.

de Anna, P., M. Dentz, A. Tartakovsky, and T. Le Borgne (2014a), The filamentary structure of mixing fronts and its control on reaction kinetics in porous media flows, *Geophys. Res. Lett.*, *41*, 4586–4593, doi:10.1002/2014GL060068.

de Anna, P., J. Jimenez-Martinez, H. Tabuteau, R. Turuban, T. Le Borgne, M. Derrien, and Y. Méheust (2014b), Mixing and reaction kinetics in porous media: An experimental pore scale quantification, *Environ. Sci. Technol.*, *48*, 508–516.

de Barros, F., M. Dentz, J. Koch, and W. Nowak (2012), Flow topology and scalar mixing in spatially heterogeneous flow field, *Geophys. Res. Lett.*, *39*, L08404, doi:10.1029/2012GL051302.

de Gennes, P. G. (1983), Hydrodynamic dispersion in unsaturated porous media, *J. Fluid Mech.*, *136*, 189–200.

de Simoni, M., J. Carrera, X. Sanchez-Vila, and A. Guadagnini (2005), A procedure for the solution of multicomponent reactive transport problems, *Water Resour. Res.*, *41*, W11410, doi:10.1029/2005WR004056.

de Simoni, M., X. Sanchez-Vila, J. Carrera, and M. Saaltink (2007), A mixing ratios-based formulation for multicomponent reactive transport, *Water Resour. Res.*, *43*, W07419, doi:10.1029/2006WR005256.

Dentz, M., T. Le Borgne, A. Englert, and B. Bijeljic (2011), Mixing, spreading and reaction in heterogeneous media: A brief review, *J. Contam. Hydrol.*, *120-121*, 1–17.

Fluhler, H., W. Durner, and M. Fluru (1996), Lateral solute mixing processes—A key for understanding field-scale transpor of water and solutes, *Geoderma*, *70*, 165–183.
Guillon, V., M. Fleury, D. Bauer, and M. Neel (2013), Superdispersion in homogeneous unsaturated porous media using NMR propagators, *Phys. Rev. E*, *87*, 043007.
Haga, D., Y. Niibori, and T. Chida (1999), Hydrodynamic dispersion and mass transfer in unsaturated flow, *Water Resour. Res.*, *35*(4), 1065–1077.
Hammel, K., and K. Roth (1998), Aproximation of asymptotic dispersivity of conservative solute in unsaturated heterogeneous media with steady state flow, *Water Resour. Res.*, *34*(4), 709–715.
Hrachowitz, M., H. Savenije, T. A. Bogaard, D. Tetzlaff, and C. Soulsby (2013), What can flux tracking teach us about water age distribution patterns and their temporal dynamics?, *Hydrol. Earth Syst. Sci.*, *17*, 533–564.
Jha, B., L. Cueto-Felgueroso, and R. Juanes (2011), Fluid mixing from viscous fingering, *Phys. Rev. Lett.*, *106*, 194502.
Kitanidis, P. K. (1994), The concept of the Dilution Index, *Water Resour. Res.*, *30*(7), 2011–2026.
Le Borgne, T., M. Dentz, D. Bolster, J. Carrera, J. R. de Dreuzy, and P. Davy (2010), Non-Fickian mixing: Temporal evolution of the scalar dissipation rate in heterogeneous porous media, *Adv. Water Res.*, *33*, 1468–1475.
Le Borgne, T., M. Dentz, and E. Villermaux (2013), Stretching, coalescence and mixing in porous media, *Phys. Rev. Lett.*, *110*, 204501.
Le Borgne, T., T. R. Ginn, and M. Dentz (2014), Impact of fluid deformation on mixing-induced chemical reactions in heterogeneous flows, *Geophys. Res. Lett.*, *41*, 7898–7906, doi:10.1002/2014GL062038.
Legout, C., J. Molenat, L. Aquilina, C. Gascuel-Odoux, M. Faucheux, Y. Fauvel, and T. Bariacn (2007), Solute transfer in the unsaturated zone-groundwater continuum of a headwater catchment, *J. Hydrol.*, *332*, 427–441.
Lenormand, R. (1990), Liquids in porous media, *J. Phys. Condens. Matter*, *2*(S), SA79.
Løvoll, G., Y. Méheust, R. Toussaint, J. Schmittbuhl, and K. J. Måløy (2004), Growth activity during fingering in a porous hele-shaw cell, *Phys. Rev. E*, *70*, 026301.
Maraqa, M., R. Wallace, and T. Voice (1997), Effects of a degree of water saturation on dispersivity and immobile water in sandy soil columns, *J. Contam. Hydrol.*, *25*, 199–218.
Méheust, Y., G. Løvoll, K. J. Måløy, and J. Schmittbuhl (2002), Interface scaling in a two-dimensional porous medium under combined viscous, gravity, and capillary effects, *Phys. Rev. E*, *66*, 051603.
Nielsen, D., M. T. van Genuchten, and J. Biggar (1986), Water flow and solute transport processes in the unsaturated zone, *Water Resour. Res.*, *22*(9S), 89S–108S, doi:10.1029/WR022i09Sp0089S.
Nutzmann, G., S. Maciejewski, and K. Joswig (2002), Estimation of water saturation dependence of dispersion in unsaturated porous media: Experiments and modelling analysis, *J. Hydrol.*, *25*, 565–576.
Ottino, J. M. (1989), *The Kinematics of Mixing: Stretching, Chaos, and Transport*, Cambridge Univ. Press, Cambridge, U. K.
Padilla, I. Y., T. C. J. Yeh, and M. H. Conklin (1999), The effect of water content on solute transport in unsaturated porous media, *Water Resour. Res.*, *35*(11), 3303–3313.
Persson, M., S. Haridy, J. Olsson, and J. Wendt (2005), Solute transport dynamics by high-resolution dye tracer experiments-image analysis and time moments, *Vadose Zone J.*, *4*, 856–865.
Raoof, A., and S. M. Hassanizadeh (2013), Saturation-dependent solute dispersivity in porous media: Pore-scale processes, *Water Resour. Res.*, *49*, 1943–1951, doi:10.1002/wrcr.20152.
Roth, K., and K. Hammel (1996), Transport of conservative chemical through an unsaturated two-dimensional Miller-similar medium with steady state flow, *Water Resour. Res.*, *32*(6), 1653–1663.
Russo, D. (1993), Stochastic modeling of solute flux in a heterogeneous partially-saturated porous formation, *Water Resour. Res.*, *29*, 1731–1744.
Russo, D. (1995a), On the velocity covariance and transport modeling in heterogeneous anisotropic porous formations: 2. Unsaturated flow, *Water Resour. Res.*, *31*, 139–145.
Russo, D. (1995b), Stochastic analysis of the velocity covariance and the displacement covariance tensors in partially saturated heterogeneous anisotropic porous formations, *Water Resour. Res.*, *31*(7), 1647–1658.
Russo, D. (2005), Stochastic analysis of solute mass flux in gravity-dominated flow through bimodal heterogeneous unsaturated formations, *Vadose Zone J.*, *4*, 939–953.
Russo, D., J. Zaidel, and A. Laufer (1994), Stochastic analysis of solute transport in partially saturated heterogeneous soil: 2. Prediction of solute spreading and breakthrough, *Water Resour. Res.*, *30*(3), 781–790.
Russo, D., A. Hadad, and A. Laufer (1998), A note on the orientation of the macrodispersion tensor in partially saturated heterogeneous porous formations, *Adv. Water Res.*, *21*(1), 63–70.
Sahimi, M. (2012), Dispersion in porous media, continuous-time random walks, and percolation, *Phys. Rev. E*, *85*, 016316.
Sato, T., H. Tanahashi, and H. A. Loáiciga (2003), Solute dispersion in a variably saturated sand, *Water Resour. Res.*, *39*(6), 1155, doi:10.1029/2002WR001649.
Simunek, J., and M. van Genuchten (2008), Modeling nonequilibrium flow and transport processes using HYDRUS, *Vadose Zone J.*, *7*, 782–797.
Tallakstad, K. T., H. A. Knudsen, T. Ramstad, G. Løvoll, K. J. Måløy, R. Toussaint, and E. G. Flekkøy (2009), Steady-state two-phase flow in porous media: Statistics and transport properties, *Phys. Rev. Lett.*, *102*, 074502.
Toride, N., M. Inoue, and F. J. Leij (2003), Hydrodynamic dispersion in an unsaturated dune sand, *Soil Sci. Soc. Am. J.*, *67*, 703–712.
Toussaint, R., K. J. Måløy, Y. Méheust, G. Løvoll, M. Jankov, G. Schäfer, and J. Schmittbuhl (2012), Two-phase flow: Structure, upscaling, and consequences for macroscopic transport properties, *Vadose Zone J.*, *11*(3), doi:10.2136/vzj2011.0123.
Ursino, N., T. Gimmi, and H. Fluhler (2001), Dilution of non-reactive tracers in variably saturated sandy structures, *Adv. Water Res.*, *24*, 877–885.
Vanderborght, J., and H. Vereecken (2007), Review of dispersivities for transport modeling in soils, *Vadose Zone J.*, *6*, 29–52.
Vanderborght, J., et al. (2001), Overview of inert tracer experiments in key belgian soil types: Relation between transport and soil morphological an hydraulic properties, *Water Resour. Res.*, *37*(12), 2837–2888.
Wildenschild, D., and K. H. Jensen (1999), Laboratory investigations of effective flow behavior in unsaturated heterogeneous sands, *Water Resour. Res.*, *35*(1), 17–27.
Willmann, M., J. Carrera, X. Sanchez-Vila, O. Silva, and M. Dentz (2010), Coupling of mass transfer and reactive transport for non-linear reactions in heterogeneous media, *Water Resour. Res.*, *46*, W07512, doi:10.1029/2009WR007739.
Zoia, A., M.-C. Néel, and A. Cortis (2010), Continuous-time random-walk model of transport in variably saturated heterogeneous porous media, *Phys. Rev. E*, *81*, 031104.